Coherent Kinetic Control over Crystal Orientation in Macroscopic Ensembles of Polymer Nanorods and Nanotubes

Martin Steinhart,* Petra Göring, Haissam Dernaika,† Munusamy Prabhukaran,† and Ulrich Gösele
Max Planck Institute of Microstructure Physics, Weinberg 2, D-6120 Halle, Germany

Elke Hempel and Thomas Thurn-Albrecht‡
Department of Physics, Martin Luther University, Hoher Weg 8, D-06120 Halle, Germany
(Received 26 January 2006; published 11 July 2006)

We show that the crystal orientation in polymer nanotubes and nanorods inside porous templates is controlled by the kinetics of nucleation and growth under 2D confinement. Two clear limiting cases are identified: In separated nanostructures, any crystal orientation allowing the growth of lamellar crystals along the pores appears statistically. If a bulklike surface film connects the nanostructures, macroscopic arrays with uniform crystal orientation are obtained, in which the dominant growth direction of the crystals is aligned with the long axes of the pores of the template.

DOI: 10.1103/PhysRevLett.97.027801 PACS numbers: 61.41.+e, 81.05.Lg, 81.07.Bc, 81.10.Fq

Polymers usually crystallize as lamellar crystals in which folded chains are oriented approximately perpendicular to the surface of the lamellae [1–3]. The typical thickness of these crystals lies in the nanometer range, while their lateral dimensions are in the micrometer range. Within the crystals, the chains adopt a helical conformation, and the growth of the lamellae proceeds in the lateral directions. On a larger scale, the lamellae are organized in spherulites, densely branched, isotropic, polycrystalline superstructures [4–6]. A variety of these semicrystalline polymers has been formed into nanotubes and nanorods using nanoporous templates [7–9]. Given the anisotropic structure of polymer crystals described above, their orientation within the nanostructure will strongly influence their optical, electronic, mechanical, and ferroelectric properties. Although in some cases strong orientation effects have been observed [10,11], little attention has been paid to the control of nucleation and crystal growth in this context. New phenomena are to be expected since two-dimensional (2D) confinement will suppress the formation of spherulitic superstructures. The situation has some similarity with crystallization under 2D and 3D confinement in microphase-separated block copolymers. In these materials, one often finds crystallization initiated by homogeneous nucleation [12]. Also, oriented crystal growth has been reported [13–15]. However, in contrast to these systems, ensembles of 1D nanostructures in porous templates can easily be connected with or separated from a bulk reservoir of the same material located on the surface of the templates. Using polyvinylidene fluoride (PVDF) as an example, we show that this is a crucial point for self-organized control of crystal orientation. In separated nanostructures, nucleation and growth happen independently within each entity. The resulting distribution of crystal orientations can be attributed to the initial formation of randomly oriented nuclei formed by homogeneous nucleation and a subsequent selection of growth directions compatible with the confinement imposed by the pore geometry. All crystal orientations that allow the lamellae to grow along the pores occur with statistical frequency, whereas other orientations are suppressed. [Fig. 1(a)]. If a bulk reservoir consisting of the same material is connected with the nanostructures, nucleation predominantly happens in the bulk. On average, the lamellae in the spherulites thus formed are oriented in such a way that the crystallographic direction with the highest growth rate (the $\langle 020 \rangle$ direction in the case of α-PVDF) points radially outwards [16,17]. Therefore, lamellae growing along the dominant growth direction are abundant at the surface of the spherulites and grow into the pores they hit, when the spherulites impinge on the surface of the template [Fig. 1(b)]. Thus, a kinetic selection mechanism in the reservoir followed by 1D growth along the pores, during which the initial orientation is maintained, results in macroscopic arrays of 1D nanostructures with uniform uniaxial crystal orientation. This kinetic "gate effect" explains the oriented crystallization recently reported for PVDF under 2D confinement [10,11].

PVDF, a semicrystalline functional polymer [18], commonly [19] crystallizes in the monoclinic, pseudo-orthorhombic α phase [20]]. The a and b axes of the unit cell lie approximately in the plane of the lamellar crystals, while the c axis stands perpendicular to this plane. We used commercially available PVDF (Aldrich, $M_w = 180\,000$ g/mol, $M_n = 71\,000$ g/mol) as received for our experiments. For the preparation of the PVDF nanostructures, the polymer was molten on the surface of ordered porous alumina with a pore depth of 100 μm and a pore diameter D_p of 35 nm [21] at a temperature of 210 °C. The nanorods formed by infiltration of the melt into the pores were connected with a ~500 μm thick PVDF film on the surface of the template and crystallized at a constant cooling rate of 1 K/min. To perform crystallization of separated nanostructures, we mechanically removed the surface film and performed a dry etching step with oxygen

 © 2006 The American Physical Society

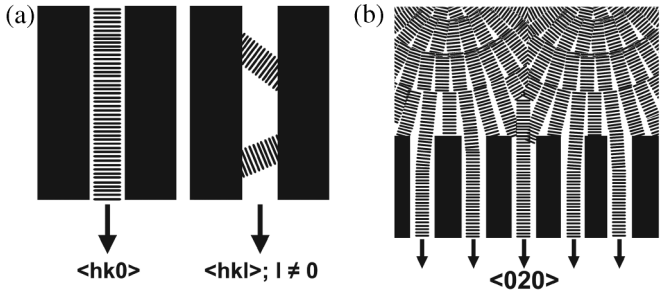

FIG. 1. Self-organized oriented crystallization of PVDF in 2D confinement (black bars: stretched PVDF chains within lamellar crystals; solid black areas: pore walls). (a) Lamellae with a $\langle hk0\rangle$ direction parallel to the pore axes grow along the pores. The pore walls stop the growth of crystals with other orientations. (b) Presence of a bulk PVDF film: Spherulites form, impinge on the template, and lamellae having the dominant $\langle 020\rangle$-growth direction aligned with the pore axes grow into the pores.

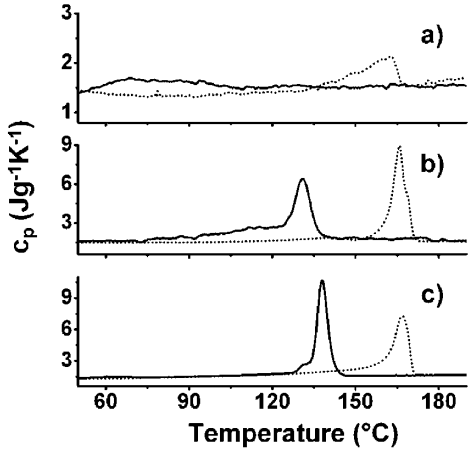

FIG. 2. DSC scans of separated PVDF nanostructures within templates (dotted curves: heating runs; solid curves: cooling runs; heating and cooling rates: 20 K/ min). (a) Nanorods (D_p = 35 nm); (b) nanotubes (D_p = 400 nm); (c) bulk PVDF. The curves were corrected by subtracting the contribution of the alumina (determined by reference measurements of empty templates).

plasma [19]. The nanorods thus separated, but still located inside the pores, were again heated to 210 °C and crystallized at a cooling rate of 1 K/ min. Following the same procedures, we prepared PVDF nanotubes inside the pores of templates with a D_p value of 400 nm [22] and a depth of 100 μm. In this case, only a thin wetting film covers the pore walls so that tubular structures with a wall thickness of ~30 nm form [9,10].

To verify the assumption of homogeneous nucleation in the separated state, differential scanning calorimetry (DSC) measurements were performed using a Perkin-Elmer DSC 7 and a Pyris DSC. Figure 2 shows DSC scans of separate PVDF nanorods [D_p = 35 nm; Fig. 2(a)] and separate PVDF nanotubes [D_p = 400 nm; Fig. 2(b)] located inside the template pores. The DSC traces of bulk PVDF shown as a reference [Fig. 2(c)] exhibit a sharp crystallization peak (onset temperature T_{onset} = 141 °C) in the cooling run and a melting peak at T_{onset} = 162 °C in the heating run. The thermal behavior of the bulk sample is typical of crystallization initiated by athermal, heterogeneous nucleation at low supercooling [23], as commonly observed for a broad range of polymeric materials. Generally, impurities act as nuclei; typical densities in PVDF were estimated to be of the order of 1 per 10^5 μm^3 [24]. However, a pore with a D_p value of 35 nm and a depth of 100 μm has only a volume of ~0.1 μm^3. In such a case, heterogeneous nucleation is not an efficient process and crystallization in an ensemble of pores has to be initiated by homogeneous nucleation [25]. The necessary high nucleation rate requires large supercooling, as is observed in the cooling run of the 35-nm sample. This sample shows a broad exothermic crystallization peak centered around 80 °C. Compared with the bulk sample, the crystallization takes place at about 60 K larger supercooling. The crystals formed at this low temperature are of lower stability, which is reflected in the melting point depression visible in the heating run of the same sample [T_{onset} = 136 °C; Fig. 2(a)]. In the cooling run of the 400-nm sample [Fig. 2(b)], crystallization starts at a temperature T_{onset} = 136 °C, considerably higher than for the 35-nm sample but still lower than in the bulk. This is in keeping with the estimate above, since a nanotube with a wall thickness of about 30 nm, an outer diameter of 400 nm, and a length of 100 μm has a volume of ~3.5 μm^3, still much less than the typical volume per heterogeneous nucleus. The shape of the crystallization peak consisting of a narrow peak with T_{onset} = 136 °C followed by a broad peak extending down to ~75 °C is not fully understood at this point. Consistent with the higher crystallization temperature, there is no clear melting point depression visible.

To analyze the crystal texture of macroscopic ensembles of aligned PVDF nanostructures located inside porous alumina, we performed wide-angle x-ray diffraction (XRD) measurements in reflection mode using a Philips X'pert MRD diffractometer with cradle and secondary monochromator for Cu K_α radiation. In the $\theta/2\theta$ geometry, θ denotes the angle between the incoming beam and the surface of the sample and 2θ the angle between the incoming and the diffracted beams. For the $\theta/2\theta$ scans, the surface of the templates was oriented perpendicular to the plane defined by the incident beam and the detector (Fig. 3). In this geometry, only crystal lattice planes oriented parallel to the surface of the template contribute to the intensity of a Bragg reflection. The scans were performed in the 2θ range from 15° to 30°, which contains four prominent reflections of α-PVDF [(100): 2θ = 17.9°; (020): 2θ = 18.3°; (110): 2θ = 20.0°; (021): 2θ = 26.6°]. For all data sets, the intensity was normalized to that of the (020) peak. Figure 4(a) shows the XRD pattern of PVDF nanorods (D_p = 35 nm) crystallized in the separated state, Fig. 4(b) that of PVDF nanotubes

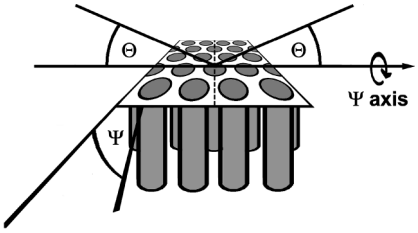

FIG. 3. Schematic diagram of the XRD setup. During a ψ scan, θ and 2θ are kept fixed and the sample is rotated about the ψ axis.

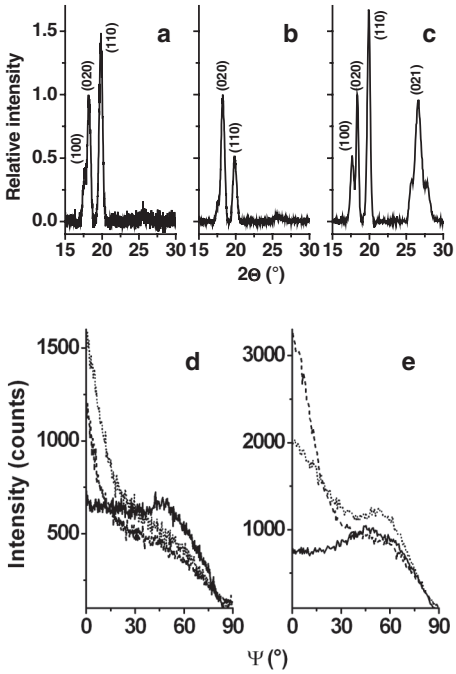

FIG. 4. XRD analysis of aligned, separated PVDF nanostructures inside the templates. (a),(b) $\theta/2\theta$ scans, intensities normalized to the (020) reflection. (a) Nanorods ($D_p = 35$ nm); (b) nanotubes ($D_p = 400$ nm); (c) bulk isotropic PVDF. (d),(e) ψ scans representing orientation distributions with respect to the template surface for specific sets of lattice planes: dashed line, (020); dotted line, (110); solid line, (021); (d) nanorods ($D_p = 35$ nm); (e) nanotubes ($D_p = 400$ nm).

($D_p = 400$ nm) crystallized in the separated state, and Fig. 4(c) that of bulk, isotropic PVDF. Most strikingly, the (021) peak at $2\theta = 26.6°$ is practically absent in Figs. 4(a) and 4(b). For the separately crystallized nanorods ($D_p = 35$ nm), the (100), (020), and (110) reflections show up with similar relative intensities as for bulk PVDF, while in the case of the PVDF nanotubes ($D_p = 400$ nm) these three reflections appear with significantly different relative intensities: The (020) peak is stronger than the (110) reflection. To analyze the distributions of the crystal orientations giving rise to the differences in the scattering patterns shown in Figs. 4(a) and 4(b), we measured ψ scans for the (020), (110), and (021) Bragg reflections. After adjusting θ and 2θ to the peak maxima of the corresponding reflection, scans were taken while tilting the samples about the ψ axis lying in the intersection of the diffraction plane and the surface of the template (Fig. 3). Neglecting effects of absorption and differences in illuminated volume, the intensity profile $I(\psi)$ is then directly proportional to the orientation distribution of the corresponding set of lattice planes. Figure 4(d) shows ψ scans measured on separately crystallized nanorods ($D_p = 35$ nm) and Fig. 4(e) on separately crystallized nanotubes ($D_p = 400$ nm). For both systems, the orientation distributions of the (020) and (110) lattice planes show pronounced maxima at $\psi = 0°$, indicating a preferred orientation of the corresponding lattice planes parallel to the surface of the samples. Consistent with the $\theta/2\theta$ scans, the curves belonging to the (021) lattice planes show no peaks at $\psi = 0°$. Instead, they exhibit maxima at $\psi \approx 45°$. This value corresponds to the angle between the (021) and (020) lattice planes and is therefore consistent with the peak of the (020) curves at $\psi = 0°$ [16,19]. In the case of the 400-nm sample, the scan belonging to the (110) reflection shows a maximum around 55°, which is coupled with the peak of the (020) curve at $\psi = 0°$ in the same way as described above.

We assume that these orientation phenomena are essentially a result of kinetic selection processes effective during crystal growth. The 35-nm rods crystallized in the separated state consist dominantly of crystals with a $\langle hk0 \rangle$ direction aligned with the long axes of the pores. Only for such an orientation are the lamellae able to grow straight along the pores. Crystal orientations with a $\langle hkl \rangle$ direction with nonzero l index parallel to the pore axis, however, are suppressed, because the lamellae cannot grow in this direction. In this way, a random orientation of homogeneous crystal nuclei is transformed into the orientation distribution analyzed above. If there is no further competition between different crystals during growth, the $\theta/2\theta$ scans should show an intensity profile similar to that of bulk isotropic PVDF, except for reflections with nonzero l index. This is consistent with our observations for the 35-nm rods. In the case of the 400-nm rods, obviously additional factors come into play, leading to an increase in intensity of the (020) reflection at the expense of the other two reflections. We suggest the following explanation: As the DSC experiments show, the nanorods crystallize at higher temperature. Because of the larger volume of the nanostructures and the lower growth rates at the high temperature of crystallization [2,17], the number of nuclei formed during the time it takes to completely crystallize a nanotube will on average be higher than in the case of the 35-nm rods. It is therefore more likely that several nuclei with different orientations, but all compatible with the selection rules discussed above, grow in competition within one pore. In such a situation, crystal faces with a higher growth rate will dominate, leading to a higher relative intensity of the (020) reflection.

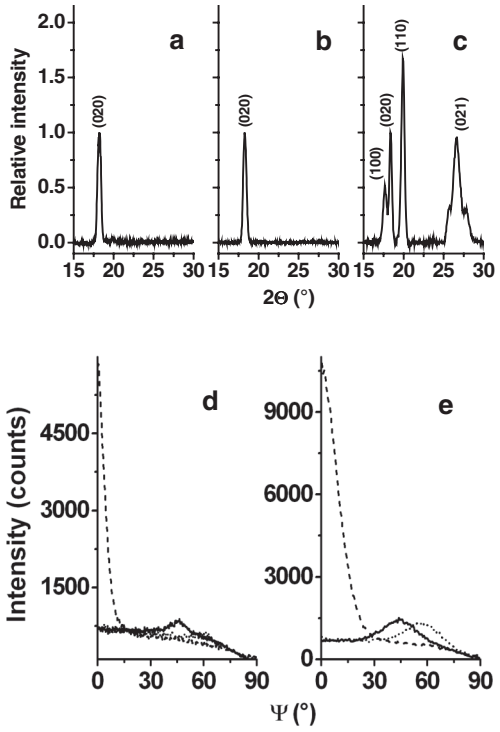

FIG. 5. XRD analysis of aligned PVDF nanostructures inside templates crystallized in the interconnected state (surface film was removed before the XRD scans). (a),(b) $\theta/2\theta$ scans, intensities normalized to the (020) reflection. (a) Nanorods (D_p = 35 nm); (b) nanotubes (D_p = 400 nm); (c) bulk isotropic PVDF. (d),(e) ψ scans representing orientation distributions with respect to the template surface for specific sets of lattice planes: dashed line, (020); dotted line, (110); solid line, (021); (d) nanorods (D_p = 35 nm); (e) nanotubes (D_p = 400 nm).

Figure 5 shows the results of the x-ray scattering experiments for the samples crystallized in the interconnected state. The surface film present during crystallization was removed before the measurements. Macroscopic ensembles of PVDF nanostructures, crystallized connected with a bulk reservoir, show a uniform, uniaxial crystal texture. Exclusively, a strong (020) peak appears in the $\theta/2\theta$ scans of both the 35-nm and the 400-nm samples [Figs. 5(a) and 5(b)]. The ψ scans for the (020) peak show again sharp maxima at $\psi = 0°$ [Figs. 5(d) and 5(e)]. The curves belonging to the (110) and (021) reflections merely exhibit maxima at 55° and 45°, respectively, corresponding to the angles between the respective lattice planes and the (020) lattice planes at $\psi = 0°$. Consistently, the ⟨020⟩ direction of PVDF is aligned with the pore axes. It is obviously the presence of the bulk reservoir which leads to the nearly complete dominance of one crystal orientation, as discussed above [Fig. 1(b)]. Additionally, our data show that the degree of crystal orientation increases with increasing confinement, as is obvious from the different full widths at half maximum (FWHM) of the peaks in the ψ scans for the (020) reflections [FWHM ≈4° for D_p = 35 nm, Fig. 5(d); FWHM ≈11° for D_p = 400 nm, Fig. 5(e)].

We have shown that the mechanisms of nucleation and growth are efficient handles to control crystal orientation within 1D nanostructures by self-organization. The 2D confinement suppresses branching as well as spherulite formation and selects specific crystal orientations during growth. This result should influence the design of nanoscaled building blocks whose performance depends on anisotropic crystal properties.

The authors thank S. Grimm and K. Herfurt for technical support, as well as the State of Saxony-Anhalt and the Volkswagen Foundation (Az.: No. I/80 780) for funding.

*Electronic address: steinhart@mpi-halle.de
†Also at Department of Physics, Martin Luther University, Hoher Weg 8, D-06120 Halle, Germany.
‡Electronic address: thurn-albrecht@physik.uni-halle.de

[1] A. Keller, Philos. Mag. **2**, 1171 (1957).
[2] G. Strobl, *The Physics of Polymers* (Springer, Berlin, 1997), 2nd ed.
[3] S. Z. D. Cheng and B. Lotz, Polymer **46**, 8662 (2005).
[4] H. D. Keith and F. J. Padden, J. Appl. Phys. **34**, 2409 (1963).
[5] D. C. Bassett and A. S. Vaughan, Polymer **26**, 717 (1985).
[6] L. Granasy *et al.*, Phys. Rev. E **72**, 011605 (2005).
[7] C. R. Martin, Science **266**, 1961 (1994).
[8] V. M. Cepak and C. R. Martin, Chem. Mater. **11**, 1363 (1999).
[9] M. Steinhart *et al.*, Science **296**, 1997 (2002).
[10] M. Steinhart *et al.*, Macromolecules **36**, 3646 (2003).
[11] Z. Hu *et al.*, Nano Lett. **5**, 1738 (2005).
[12] Y.-L. Loo, R. A. Register, and A. J. Ryan, Phys. Rev. Lett. **84**, 4120 (2000).
[13] D. J. Quiram, R. A. Register, G. R. Marchand, and D. H. Adamson, Macromolecules **31**, 4891 (1998).
[14] L. Zhu *et al.*, J. Am. Chem. Soc. **122**, 5957 (2000).
[15] Y.-L. Loo, R. A. Register, A. J. Ryan, and G. T. Dee, Macromolecules **34**, 8968 (2001).
[16] A. J. Lovinger and T. T. Wang, Polymer **20**, 725 (1979).
[17] A. J. Lovinger, J. Polym. Sci., Polym. Phys. Ed. **18**, 793 (1980).
[18] A. J. Lovinger, Science **220**, 1115 (1983).
[19] See EPAPS Document No. E-PRLTAO-97-032629 for a scanning electron micrograph of a cleaned template surface, as well as for additional information on the crystallization kinetics of PVDF and the XRD setup. For more information on EPAPS, see http://www.aip.org/pubservs/epaps.html.
[20] R. Hasegawa, Y. Takahashi, Y. Chatani, and H. Tadokoro, Polym. J. **3**, 600 (1972).
[21] H. Masuda and K. Fukuda, Science **268**, 1466 (1995).
[22] H. Masuda, K. Yada, and A. Osaka, Jpn. J. Appl. Phys. 2, Lett. **37**, L1340 (1998).
[23] D. Turnbull, J. Chem. Phys. **18**, 198 (1950).
[24] S. Schneider, X. Drujon, B. Lotz, and J. C. Wittmann, Polymer **42**, 8787 (2001).
[25] M. V. Massa and K. Dalnoki-Verres, Phys. Rev. Lett. **92**, 255509 (2004).